Research Article

Luping Wang, Haote Han, Jiahui Ma, Yue Feng, Zhuo Han, Vinesh Maharaj, Jingkui Tian, Wei Zhu, Shouxin Li* and Xiying Shao*

Identification of hypoxia-immune-related signatures for predicting immune efficacy in triple-negative breast cancer

https://doi.org/10.1515/oncologie-2023-0539
Received November 21, 2023; accepted February 2, 2024;
published online February 28, 2024

Abstract

Objectives: The therapeutic effect against triple-negative breast cancer (TNBC) varies among individuals. Finding signatures to predict immune efficacy is particularly urgent. Considering the connection between the microenvironment and hypoxia, hypoxia-related signatures could be more effective. Therefore, in this study, we aimed sought to construct a hypoxia-immune-related prediction model for breast cancer and identify therapeutic targets.
Methods: Immune and hypoxia status in the TNBC microenvironment were investigated using single-sample Gene Set Enrichment Analysis (ssGSEA) and Uniform Manifold Approximation and Projection (UMAP). The least absolute shrinkage and selection operator (LASSO) and multivariate Cox regression analysis were employed to build a prognostic model based on hypoxia-immune-related differentially expressed genes. The Cancer Genome Atlas (TCGA) cohort, real-time quantitative polymerase chain reaction (qRT-PCR), and immunofluorescence staining were utilized to analyze the expression differences. Tumor immune dysfunction and exclusion indexes were used to indicate the effect of immunotherapy.
Results: We identified 11 signatures related to hypoxia and immunity. Among these genes, C-X-C motif chemokine ligand (CXCL) 9, 10, and 11 were up-regulated in TNBC tissues compared to normal tissues. Furthermore, CXCL9, 10, 11, and 13 were found to enhance the effect of immunotherapy.
Conclusions: These findings suggest the value of the hypoxia-immune-related prognostic model for estimating the risk in patients with TNBC, and CXCL9, 10, 11, and 13 are potential targets to overcome immune resistance in TNBC.

Keywords: triple-negative breast cancer; prognostic model; CXC chemokines; hypoxia; immune infiltration; tumor microenvironment

Introduction

Breast cancer (BC), one of the most common mammary cancers, accounts for 31 % of female cancers, making it a leading cause of cancer death [1, 2]. BC patients benefit from a series of therapies, such as including targeted therapy, hormonal therapy, radiation therapy, surgery, and chemotherapy [3]. Triple-negative breast cancer (TNBC), a subtype comprising 15–20 % of BC, is characterized by the negative expression of estrogen receptor (ER), progesterone receptor (PR), and human epidermal growth factor receptor 2 (HER2) [4]. TNBC exhibits higher aggression, relapse, and mortality rates compared to other BC subtypes. Unlike other subtypes, patients with TNBC do not benefit from hormonal therapy and HER2-targeted therapies [5–8]. Recently, immunotherapies such as chimeric antigen receptor T-cell immunotherapy (CAR-T) and programmed cell death 1 ligand 1 (PD-L1) treatment have been applied to TNBC, potentially

Luping Wang and Haote Han contributed equally to this work.

***Corresponding authors: Shouxin Li**, Chinese Academy of Sciences, Hangzhou Institute of Medicine, Hangzhou 310002, China, E-mail: yihelaosou@163.com; and **Xiying Shao**, Department of Breast Medical Oncology, Zhejiang University of Traditional Chinese Medicine Affiliated Cancer Hospital, Hangzhou 31000, China, E-mail: shaoxy@zjcc.org.cn.
Luping Wang, College of Biomedical Engineering & Instrument Science, Zhejiang University, Hangzhou 310027, China; and Chinese Academy of Sciences, Hangzhou Institute of Medicine, Hangzhou 310002, China. https://orcid.org/0000-0002-5029-0718
Haote Han, College of Biomedical Engineering & Instrument Science, Zhejiang University, Hangzhou 310027, China
Jiahui Ma, Yue Feng, Zhuo Han, Jingkui Tian and Wei Zhu, Chinese Academy of Sciences, Hangzhou Institute of Medicine, Hangzhou 310002, China
Vinesh Maharaj, Department of Chemistry, Faculty of Natural and Agricultural Science, University of Pretoria, Private Bag x20, Pretoria 0028, South Africa

overcoming the limitations of traditional therapies [9]. Therefore, exploring unconventional therapeutic targets for TNBC is crucial.

Hypoxia, a critical microenvironmental factor, promotes tumor proliferation and progression. BC tissues carry only approximately 1 % oxygen compared to 8 % oxygen in normal breast tissue [10]. Hypoxia has been shown to suppress immunity in the tumor microenvironment (TME) by inhibiting the activation and proliferation of T cells [11, 12].

Tumor cells secrete chemokines to facilitate their growth, metastasis, angiogenesis, and immune escape [13, 14]. Accumulating evidence supports the importance of CXC chemokines in angiogenesis and metastasis [15]. Members of the CXC chemokine family (CXCL1-3 and CXCL5-8) containing the ELR motif (Glu-Leu-Arg sequence) are angiogenic factors, whereas those without the ELR motif (ELR-negative, CXCL4, and CXCL9-16) are potent inhibitors of angiogenesis [16–19]. Several reports have revealed that CXCL1 is expressed lower in BC [20]. Meanwhile, ELR-positive CXCL2, 3, 5, 6, 7 and 8 are considered as diagnostic and prognostic markers for BC [21]. CXCL14 has also been reported to promote the invasion of BC [22]. As for the receptors, CXCR1 and CXCR2 have been found to mediate BC proliferation and progression with the interaction of CXCL8 [23, 24]. Activation of the CXCR4/CXCL12 complex has been proved to have a strict one-to-one binding affinity and made CXCR4 a treating target for BC [25–27]. Furthermore, the CXCR4/CXCL12 interaction has been reported in TNBC cells, mediating metastasis and progression [28]. Besides, the CXCL8-CXCR1/2 signaling axis plays an important role in inflammation and the TME in BC [29]. However, few reports have elaborated on CXCLs and their interactions with receptors in TNBC. The biological function of CXCL 9–11, also crucial members of the CXC family, remains unclear in BC or TNBC.

Using genetic and bioinformatics analyses, we constructed a prediction model by selecting hypoxia- and immune infiltration-associated genes. Subsequently, we evaluated the role of CXC chemokines as potential targets to overcome immune resistance and verified in TNBC and normal tissues.

Patients and methods

Major reagents

The following regents were procured for the study: GeoMx Immune Cell Profiling Panel Human Protein Core for nCounter kit, GeoMx Hyb Code Pack Protein kit, GeoMx Nuclear Stain Morphology kit, GeoMx Protein Slide Prep kit, GeoMx Hyb Buffer, GeoMx Digital Spatial Profiler (DSP) Collection Plates 96, GeoMx DSP Instrument Buffer Kit and nCounter Master Kit were purchased from NanoString Technologies (WA, USA). Anti-CXCL9, anti-IP10, anti-CXCL11, and anti-BCA1 antibodies were procured from Abcam (Cambridge, UK). Horseradish peroxidase (HRP)-conjugated mouse anti-rabbit IgG antibody was obtained from Santa Cruz Biotechnology (TX, USA).

Tissues

TNBC tissues were provided by the Zhejiang Cancer Hospital and used for experimental verification, with approval from the Zhejiang Cancer Hospital Ethics Committee (No. IRB-2021-19). In this study, nine para-carcinoma tissues and 15 tumor tissues were obtained from 15 participants. Participants with TNBC (HER2-, PR- and ER-) were included in the cohort, whereas participants with other BC subtypes were excluded. Para-carcinoma tissues were collected with paired tumor tissues (6 of the tumor tissues were not paired with para-carcinoma). All the participants were female and provided written informed consent. Due to restrictions, obtaining more tissues was not feasible.

Patient cohort and data preparation using public databases

This study included 320 patients from the Gene Expression Omnibus (GEO, https://www.ncbi.nlm.nih.gov/geo/) database (GSE202203). External validations were performed on two cohorts: GSE103091 and TNBC data screening from the Cancer Genome Atlas (TCGA, https://portal.gdc.cancer.gov/) database.

Identification of immune status and differentially expressed genes (DEGs) related to immune infiltration

The scores of 28 types of immune cells were calculated using the single sample Gene Set Enrichment Analysis (ssGSEA) algorithm of R (version 4.3.1) package “GSVA”. Based on these scores, patients were divided into two clusters using Uniform Manifold Approximation and Projection (UMAP) of R package “umapr”. The DESeq2 algorithm was applied to identify differentially expressed genes (DEGs) ($p<0.05$ and absolute $\log_2$ (fold change)>0.5). High- and low-immune groups were identified based on the pathways enriched by DEGs.

Identification of hypoxia status and DEGs related to hypoxia

The hypoxia degree of patients was explored using the R package “GSVA” based on hypoxia markers downloaded from the Molecular Signatures Database (MSigDB, https://www.gsea-msigdb.org/gsea/msigdb). Two groups of patients were then divided into high- and low-risk groups based on the optimal cutting point, which was determined by maximally selected rank statistics using the “survival” and “survminer” R packages.

Prediction model of TNBC based on hypoxia-immune-related DEGs

Protective and risky DEGs related to hypoxia and immune responses were identified through univariate Cox regression analysis (UCRA) using the R package "ezcox". These DEGs were further screened using Venn analysis (R package "VennDiagram"). Subsequently, the optimal variables were predicted using least absolute shrinkage and selection operator (LASSO) regression analysis (R package "glmnet"). Multivariate Cox regression analysis (MCRA) was further performed to identify signature genes for the TNBC prediction model using the R packages "ezcox" and "forestplot". For each patient, the risk score was calculated using the formula in Equation (1):

$$\text{Risk score} = \sum_{i=1}^{n} \text{coefficient} \times \text{expression of characteristic gene}_i \quad (1)$$

Equation (1) formula for calculating the risk score of patients.

Based on the risk scores, patients were classified into high- and low-risk groups according to the optional cutting point.

Tumor Immune Dysfunction and Exclusion (TIDE)

TIDE (http://tide.dfci.harvard.edu) is a platform that evaluates the potential for immune evasion based on the gene expression profiles of cancer samples [30]. In conjunction with TIDE, we assessed immune evasion abilities using TNBC data from GSE202203. These indexes were instrumental in predicting the response to immune checkpoint blockade (ICBs).

Digital spatial profiler (DSP)

DSP was performed using the GeoMx digital spatial profiler platform (NanoString Technologies). The DSP process strictly adhered to the user guide of the GeoMx instrument. Briefly, slides, after deparaffined and subjected to antigen retrieval procedures, were co-incubated with three fluorescent-labeled visualization antibodies targeting immune cells (Table 1). After region of interest (ROI) selection, DSP barcodes were released from each ROI upon UV exposure. Released tags were quantitated with the NanoString GeoMx-nCounter DSP instrument (NanoString Technologies) and were then hybridized and counted on the nCounter system (NanoString Technologies).

RNA isolation and quantitative real-time polymerase chain reaction (qRT-PCR) analysis

Initially, qRT-PCR was used to investigate the mRNA levels of CXC chemokines (CXCL1-7, 9–14) in CTs and NATs. Total RNA was isolated from CTs and NATs using the RNAprep pure Tissue kit (TIANGEN, Beijing, China) according to the manufacturer's instructions. Subsequently, cDNA was synthesized using a 5 × All-In-One RT MasterMix kit (Applied Biological Materials Inc., Vancouver, Canada) following the manufacturer's instructions. Briefly, qRT-PCR was performed on a Thermal Cycler system (Bio-Rad Laboratories Inc., CA, USA) with the following amplification steps: 94 °C for 4 min, followed by 40 cycles at 94 °C for 60s, 60°C–65 °C for 30s, 72 °C for 2 min, and 72 °C for 5 min using the BlasTaq 2× qPCR MasterMix kit (Applied Biological Materials Inc., Vancouver, Canada). Primers were designed using Primer Premier 5.064 software, and the primer sequences are as the following:

CXCL1: forward primer, 5′-AGTGGCACTGCTGCTCCT-3′; reverse primer, 5′-TGGATGTTCTTGGGGTGAAT-3′. CXCL2: forward primer, 5′-CTGCTCCTGCTCCTGGTG-3′; reverse primer, 5′-AGGGTCTGCAAGCACTGG-3′. CXCL3: forward primer, 5′-CGCCCAAACCGAAGTCATAG-3′; reverse primer, 5′-GCTCCCCTTGTTCAGTATCTTTT-3′. CXCL4: forward primer, 5′-GCGGTTACCATGGAGGGGAT-3′; reverse primer, 5′-GCGGTTACCATGGAGGGGAT-3′. CXCL5: forward primer, 5′-AGCTGCGTTGCGTTTGTTTAC-3′; reverse primer, 5′-TGGCGAACACTTGCAGATTAC-3′. CXCL6: forward primer, 5′-AGAGCTGCGTTGCACTTGTT-3′; reverse primer, 5′-GCAGTTTACCAATCGTTTTGGGG-3′. CXCL7: forward primer, 5′-GTAACAGTGCGAGACCACTTC-3′; reverse primer, 5′-CTTTGCCTTTCGCCAAGTTTC-3′. CXCL9: forward primer, 5′-CCAGTAGTGAGAAAGGGTCGC-3′; reverse primer, 5′-AGGGCTTGGGGCAAATTGTT-3′. CXCL10: forward primer, 5′-GTGGCATTCAAGGAGTACCTC-3′; reverse primer, 5′-TGATGGCCTTCGATTCTGGATT-3′. CXCL11: forward primer, 5′-GACGCTGTCTTTGCATAGGC-3′; reverse primer, 5′-GGATTTAGGCATCGTTGTCCTTT-3′. CXCL12: forward primer, 5′-ATTCTCAACACTCCAAACTGTGC-3′; reverse primer, 5′-ACTTTAGCTTCGGGTCAATGC-3′. CXCL13: forward primer, 5′-GCTTGAGGTGTAGATGTGTCC-3′; reverse primer, 5′-CCCACGGGGCAAGATTTGAA-3′. CXCL14: forward primer, 5′-CGCTACAGCGACGTGAAGAA-3′; reverse primer, 5′-GTTCCAGGCGTTGTACCAC-3′. GAPDH: forward primer, 5′-ACTCAGGAGAGTGTTTCCTCG-3′; reverse primer, 5′-TTTGCCGTGAGTGGAGTCAT-3′.

Table 1: Target proteins within Digital Spatial Profiler (DSP) modules.

Target group membership/s	Target name
Total immune	CD45
Checkpoint, T cell activation, T cells, Th cells	CTLA4
Housekeepers	GAPDH
Checkpoint, myeloid activation	PD-L1
Housekeepers	S6
Background	Ms IgG2a
Proliferation	Ki-67
Checkpoint, T cell activation, T cells	PD-1
MHC2, antigen presentation	HLA-DR
M2 macrophage, macrophage, myeloid	CD68
DC, myeloid	CD11c
B cells	CD20
Tumor, antigen presentation	Beta-2-microglobulin
T cells	CD3
CD8 T cells, T cells	CD8
Tumor, epithelial	PanCk
Stroma	SMA
Housekeepers	Histone H3
Stroma, fibroblasts	Fibronectin
T cell activation, cytotoxicity	GZMB
Background	Ms IgG1
NK cells	CD56
Background	Rb IgG
T cells, Th cells, myeloid	CD4

The correlation analysis of housekeeper and background targets was performed in GraphPad Prism 9.5. After normalization using IgG (Rb IgG, Ms IgG2a, and Ms IgG1) proteins, the levels of immune-related proteins were visualized in a heatmap. Differentially expressed proteins (DEPs) in cancer tissues (CTs) versus normal adjacent tissues (NATs) were analyzed using the R package "limma", and visualized using volcano maps.

Relative gene expression levels was calculated using the $2^{-\Delta\Delta CT}$ method [31].

Immunofluorescence staining assay

Slides, after deparaffinization and antigen retrieval procedures were incubated overnight at 4 °C with specific primary antibodies. Following three washes with phosphate-buffered saline (PBS)-Triton (0.01 M PBS with 0.5 % Triton, pH 7.4), samples were incubated with immunofluorescence secondary antibodies for 1 h in a dark environment. The nuclei were stained with 2-(4-amidinophenyl)-6-indolecarbamidine dihydrochloride (DAPI) solution (10 μg/mL) obtained from Solarbio (Beijing, China) for 5 min at room temperature. Subsequently, images were captured using the SLIDEVIEW VS200 system (Olympus, Tokyo, Japan). The fluorescence intensity was quantified using ImageJ Software (version v1.8.0, University of Wisconsin-Madison, USA).

Results

Immune status and DEGs related to immunity in TNBC

Transcriptome expression profiles of immune markers revealed distinct expression patterns in TNBC compared to other types of BC (Supplementary Figure 1A and B). The top 40 up- and down-regulated immune DEGs included six chemokines (CCL14, CCL7, CXCL10, CXCL11, CCL11, CCL20, and CXCL9, Supplementary Figure 1C).

Patients were clustered into Clusters 1 and 2 based on the expression of immune genes (Figure 1A). Cluster 2 exhibited a higher immune status, with up-regulated DEGs enriched in pathways such as cytokine-cytokine receptor interaction, chemokine signaling pathway, B cell receptor signaling pathway, and T cell receptor signaling pathway (Figure 1B). Consequently, Cluster 2 was designated as the high-immune group, whereas Cluster 1 was considered the low-immune group. The high-immune group exhibited higher survival rate and increased immune infiltration compared to the low-immune group (Figure 1C and D).

Hypoxia status and DEGs related to hypoxia in TNBC

Transcriptome expression profiles of hypoxia markers indicated the differences between TNBC and other types of BC (Supplementary Figure 1A and B). The top 40 up-regulated hypoxia DEGs were predominantly related to metabolism such as carbon metabolism, glycolysis/gluconeogenesis, and central carbon metabolism in cancer (Supplementary Figure 1D).

Patients were divided into high- and low-hypoxia groups based on the hypoxia score calculated by ssGSEA (Figure 1E). The high-hypoxia group characterized by higher expression levels of hypoxia markers exhibited a worse survival rate (Figure 1F and G).

Hypoxia-immune-related DEGs in TNBC

Patients were categorized into four groups (Hyp&Imm_high, Hyp&Imm_low, Hyp_high&Imm_low, and Hyp_low&Imm_high) based on the above immune and hypoxia grouping mentioned earlier. Patients with high immune and low hypoxia status (Hyp_low&Imm_high) exhibited significantly higher survival rates than patients in the other three groups (Figure 1H).

UCRA identified 14 protective and 81 risky immune-hypoxia-related DEGs (Figure 1I). Protective genes were primarily involved in pathways related to T cells, and biological processes associated with T and natural killer (NK) cells, whereas risk genes were mainly enriched in pathways related to hypoxia, glycolysis, angiogenesis, and apoptosis (Figure 1J).

Hypoxia-immune-related prognostic prediction model of TNBC

Using the identified 95 hypoxia-immune-related genes, 63 genes were selected through UCRA for LASSO regression analysis (Figure 2A and B). Subsequently, 11 characteristic genes were identified through MCRA (Figure 2C). Of these 11 genes, NELL2 (coefficient=−0.002) and MGARP (coefficient=−0.055) were protective, whereas STMN2 (coefficient=0.002), WFDC1 (coefficient=0.001), FIBCD1 (coefficient=0), NIPAL1 (coefficient=0.001), CABP7 (coefficient=0.003), LY6H (coefficient=0.004), RPRML (coefficient=0.001), MRAP2 (coefficient=0.001), and CLCNKA (coefficient=0.022) were considered risk genes. Except for CABP7, all these 11 characteristic genes, significantly influenced the survival rate of TNBC patients (Supplementary Figure 2). Specifically, patients with high expression levels of the two protective genes had significantly higher survival rates, while those with high expression levels of STMN2, WFDC1, FIBCD1, NIPAL1, LY6H, RPRML, MRAP2, and CLCNKA exhibited significantly lower survival rates. Risk scores of patients with TNBC were calculated using these 11 characteristic genes based on Equation (1). Patients were then divided into high- and low-risk groups according to their risk scores (Figure 2D). The low-risk group exhibited a significantly higher survival rate than the high-risk group (Figure 2E).

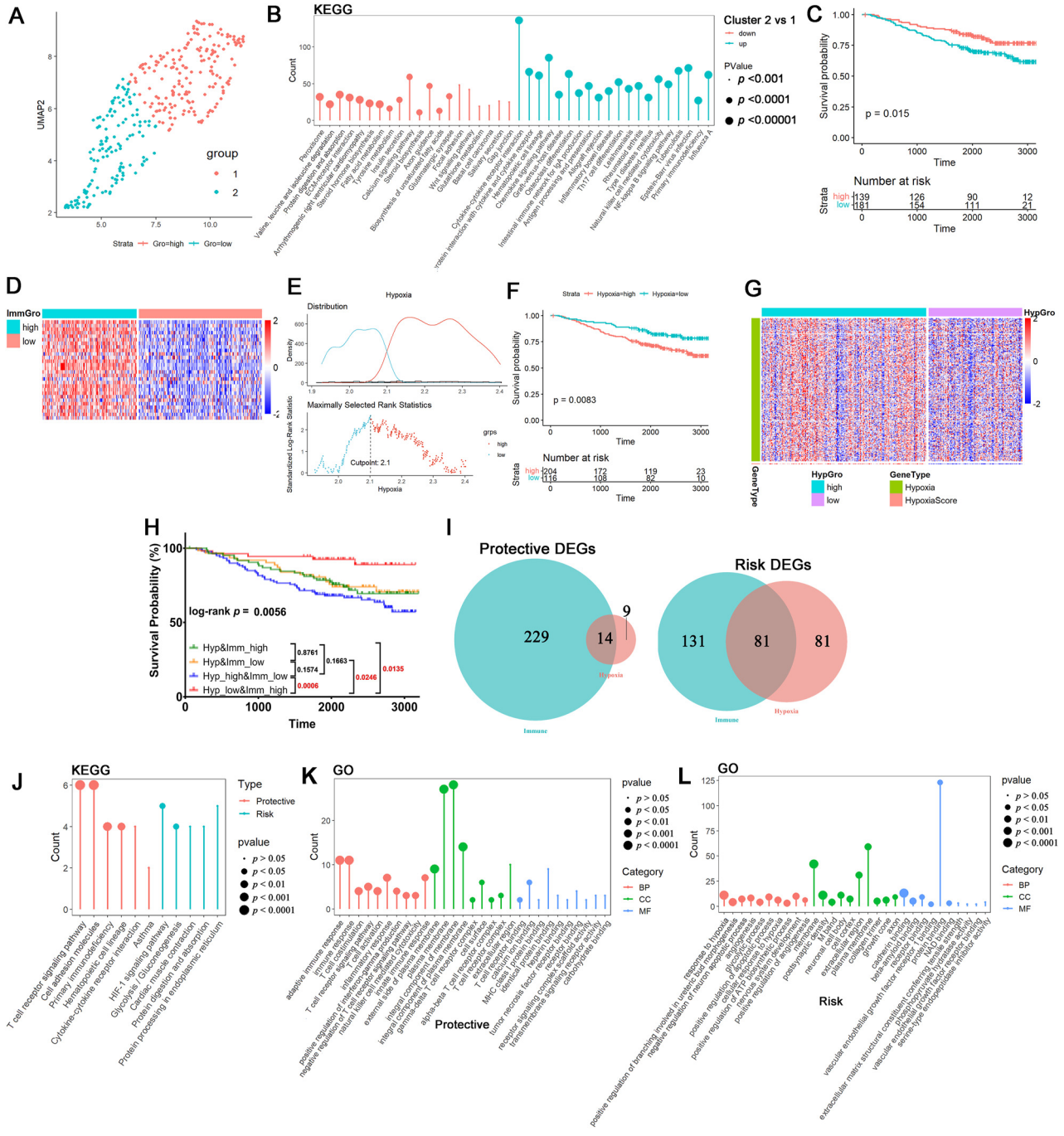

Figure 1: Grouping of patients according to the marker gene set of immune and hypoxia. (A) The UMAP algorithm classified patients with TNBC into two clusters based on the ssGSEA scores of immune cells. (B) Functional enrichment analysis of DEGs between cluster 2 (vs. cluster 1). (C) Kaplan–Meier plot of overall survival between low- and high-immune groups. (D) The profile of ssGSEA scores of immune cells between high- and low-immune groups was visualized in a heatmap. (E) The cut-off points with the maximum standard log-rank statistic based on hypoxia scores calculated using ssGSEA. (F) Kaplan–Meier plot of overall survival between low- and high-hypoxia groups. (G) The profile of hypoxia genes and hypoxia score between high- and low-hypoxia groups were visualized in a heatmap. (H) Kaplan–Meier plot of overall survival among Hyp&Imm_high (high-hypoxia and high-immune), Hyp&Immune_low (low-hypoxia and low-immune), Hyp_high&Imm_low (high-hypoxia and low-immune), and Hyp_low&Imm_high (low-hypoxia and high-immune) groups. (I) Protective (coefficient>0, and p<0.05) and risky (coefficient<0, and p<0.05) DEGs related to hypoxia and immune shown in Venn diagrams. Results of Kyoto Encyclopedia of Genes and Genomes (KEGG) (J) and Gene Ontology (GO) (K, and L) functional enrichment analysis of hypoxia-immune- related protective and risky DEGs.

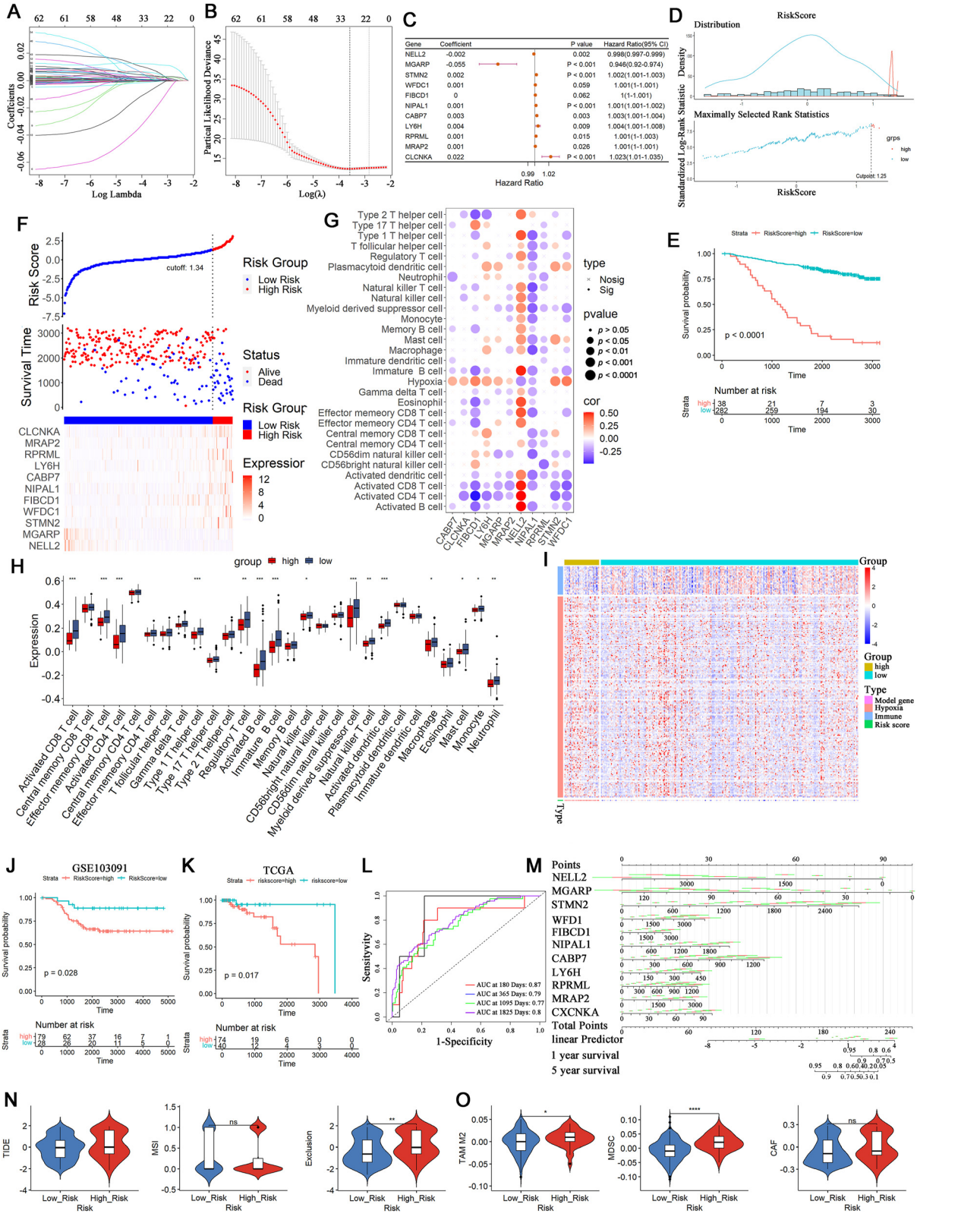

Figure 2: Constructing a prognostic survival model of patients with TNBC. (A) LASSO coefficient profiles of 63 screened DEGs. (B) Three-fold cross-validation of LASSO analysis. (C) Forest plot of the prognostic effects of 11 DEGs with p<0.05 on a multivariate Cox regression analysis, out of 15 DEGs screened from LASSO analysis. (D) Determination of cut-off points with the maximum standard log-rank statistic based on risk scores calculated using multivariate Cox regression results of 11 DEGs. (E) Kaplan–Meier plot of overall survival between low and high-risk score groups. (F) Distribution of patients, scatter plot of patient survival and expression profiles of model genes with increased risk scores in the two groups. (G) Heatmap showing the

Compared to the low-risk group, the high-risk group had a higher proportion of deaths, higher expression of risk signatures, and lower expression of protective signatures (Figure 2F). The protective gene, NELL2, was positively correlated with immune cells and negatively correlated with hypoxia, whereas the opposite was observed for another protective gene, MGARP (Figure 2G). All risk genes were mainly negatively correlated with immune cells and positively correlated with hypoxia except NIPAL1. Additionally, the high-risk group had lower immune infiltration and higher hypoxia and risk scores (Figure 2I–H).

To assess the value of the prognostic prediction model, the receiver operating characteristic (ROC) curves of the area under the curve (AUCs) within 180, 365, 1095, and 1825 days were all higher than 0.75 in GSE202203 (Figure 2L). A nomogram for 1- and 5-year overall survival predictions was developed based on the model genes (Figure 2M). Further validation of the prediction value through overall survival analyses was conducted in GSE103091 and TCGA cohorts, both of which revealed that the low-risk group had a significantly higher survival rate (Figure 2J and K). Moreover, the high-risk group exhibited a higher T cell exclusion, immunosuppressive cells, the infiltrations of the M2 subtype of tumor-associated macrophages (M2 TAMs), and myeloid-derived suppressor cells (MDSCs). Consequently, the high-risk group showed a worse response to immunotherapy (Figure 2N and O).

The results presented in Figure 2 suggest the predictive value of our prognostic prediction model.

CXCL9, 10, 11, and 13 are immune-related chemokines and protective factors in TNBC

According to Figure 1B, CXC chemokines were implicated 8 of the 20 KEGG pathways enriched by over-expressed DEGs in the high-immune group. Additionally, in the high-risk group, 30 GO and 20 KEGG pathways were enriched by down-regulated DEGs correlated with model genes, 13 of which involved CXC chemokines (Figure 3A and Supplementary Figure 3). Survival analysis revealed that patients with high expression of CXCL1, 2, 9, 10, 11, 12, 13, and 14 exhibited higher survival rates (Supplementary Figure 4).

Correlation analysis revealed that CXCL9, 10, 11, and 13 were positively correlated with the protective model gene NELL2 and most immune cells, and negatively correlated with most risk model genes (Figure 3B and C). And CXCL9 and CXCL13 were negatively correlated with hypoxia. These results suggested that CXCL9, 10, 11, and 13 were protective genes in TNBC.

Boxplots of CXC chemokines in the high-risk group vs. the low-risk group demonstrated that only CXCL9, 10, 11, and 13 were significantly down-regulated (Figure 3D). According to the TIDE analysis (Figure 3E), high-CXCL9 and high-CXCL13 groups had significantly lower MSI scores, exclusion score, TAM M2 score, MDSC score, and CAF score. Patients with low CXCL10 expression had worse immunotherapy responses. All the indexes, except MDSC, had lower scores in the high-CXCL11 group. Therefore, CXCL9, 10, 11, and 13 may contribute to the clinical efficacy of ICB therapy, especially in high-risk populations.

CXC chemokines differentially expressed in patients with TNBC compared to normal tissues

CXC chemokines in the TME could modulate immune cell trafficking and regulate tumor cell activity. Compared to NTs, the depression of CXCL2, 4, 7, 12, and 14 and the increment of CXCL8-11, and 13 were revealed in the TNBC dataset from TCGA (Supplementary Figure 5A).

Subsequently, we evaluated the mRNA levels of CXC chemokines in clinical samples (Supplementary Figure 5B). The up-regulation of CXCL9 and 10 and down-regulation of CXCL2 and 12 were evident in TNBC vs. NATs. However, there was no significant difference in CXCL13 expression between TNBC and NATs.

Furthermore, we also analyzed the protein levels of CXCL9, 10 (IP10), CXCL11 and 13 (BCA1) using immunofluorescence staining (Figure 4). As expected, CXCL9, 10 and 11 were significantly up-regulated in TNBC compared to NATs. However, the up-regulation of CXCL13 was not significant. Up-regulating the CXCL13 may be helpful for improving the condition of patients with TNBC.

correlation between model genes and 28 immune cells as well as hypoxia. (H) Box plots of the expression of immune cells in high- and low-risk groups. (I) Visualization of the expression values of immune cells, hypoxia marker genes, model genes, and risk scores for each sample in a heatmap. (J) Kaplan–Meier plot of overall survival between high- and low-risk groups in the GSE103091 validation cohort. (K) Kaplan–Meier plot of overall survival between high- and low-risk groups in the TCGA validation cohort. (L) The ROC curve evaluating the predictive value of the model for the prognosis of TNBC patients at different time points. (M) Nomogram for 1- and 5-year overall survival is based on the Cox model. (N) Differences in relevant indexes of immunotherapy prediction (TIDE score, microsatellite instability (MSI) score, and immune exclusion) between low- and high-risk groups, where "ns" indicates non-significant, *p<0.05, **p<0.01 and ****p<0.0001. (O) Differences in the scores of immunosuppressive cells, M2 subtype of tumor-associated macrophages (TAM M2), myeloid-derived suppressor cell (MDSC) and cancer-associated fibroblast (CAF) scores between low- and high-risk groups.

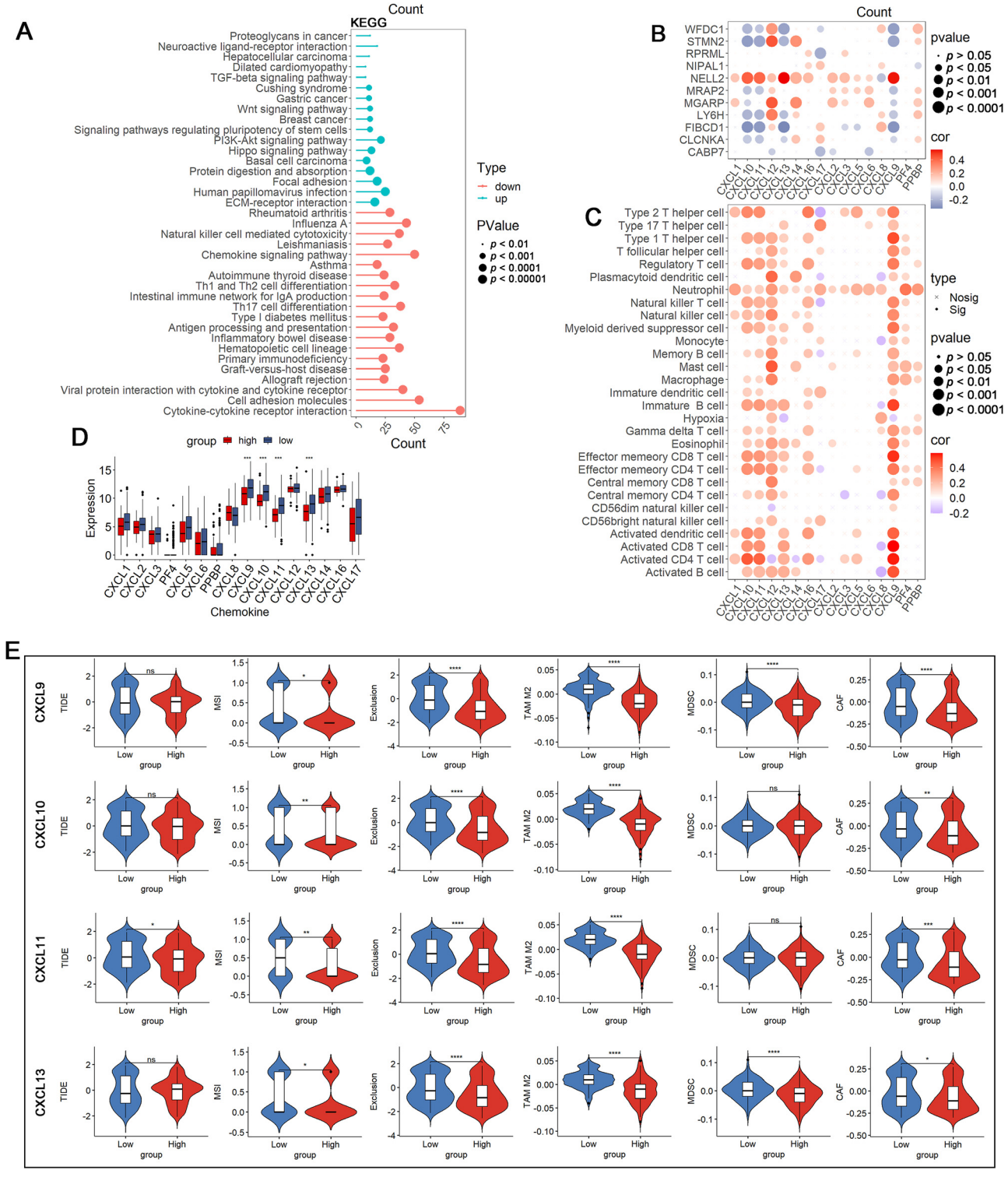

Figure 3: CXCL9, 10, 11, and 13 are protective genes in TNBC. (A) After correlation, KEGG functional enrichment analysis of DEGs correlated to model genes were conducted and compared between high- and low-risk groups. (B) Correlation between CXCL chemokines and model genes. (C) Correlation between CXCL chemokines and immune cells as well as hypoxia. (D) Box plot of the expression of CXC chemokines in high- and low-risk groups. (E) The difference of relevant indexes of immunotherapy prediction (TIDE score, MSI score, immune exclusion, and M2 type macrophage infiltration), MDSC, and CAF score between high- and low-expression of CXCL9, CXCL10, CXCL11, and CXCL13 respectively. The “ns”, “*”, “**”, “***”, and “****” indicate statistical significance at p>0.05, p<0.05, p<0.01, p<0.001, and p<0.0001, respectively.

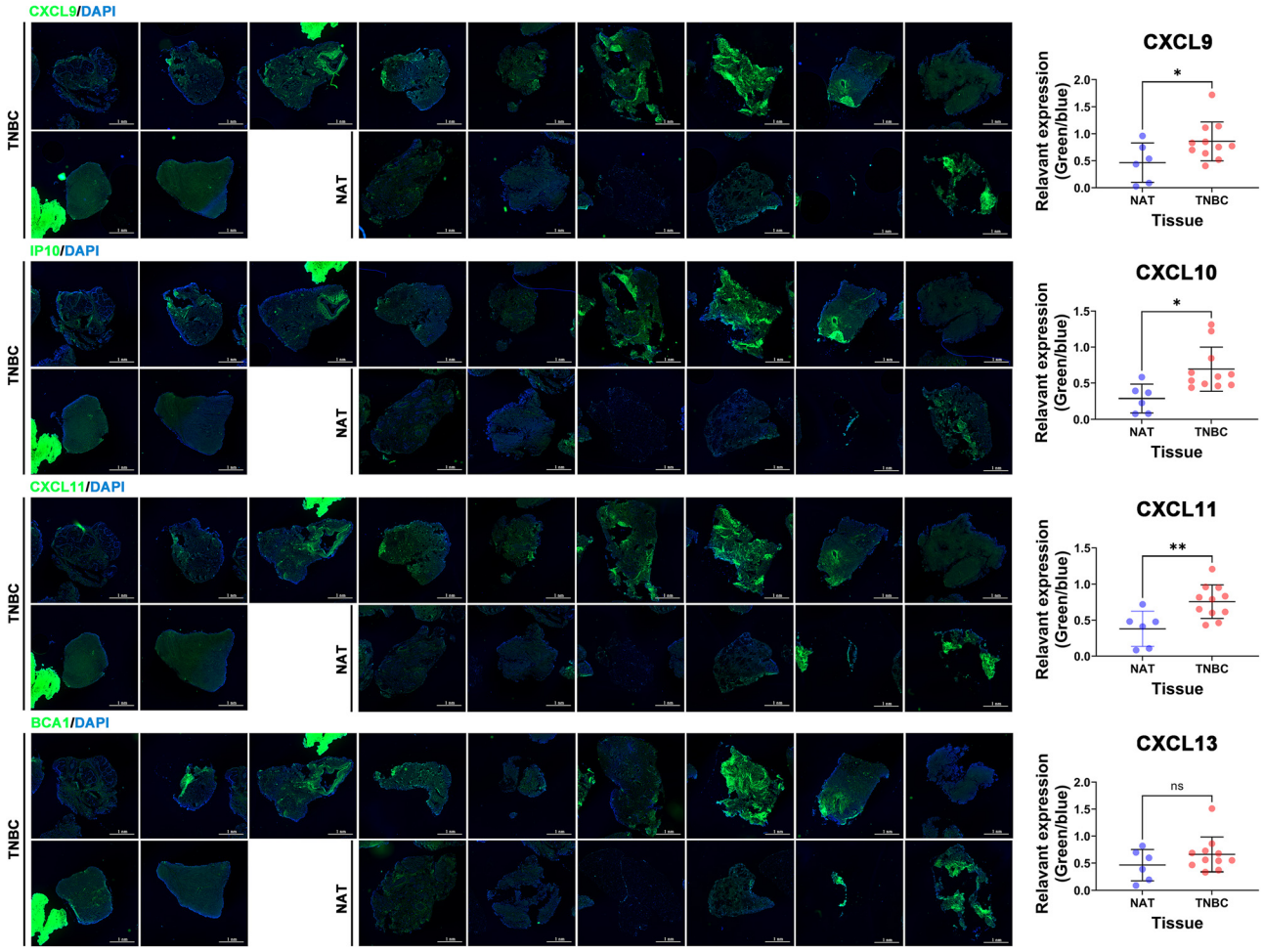

Figure 4: Analysis of protein levels of CXC chemokines in TNBC vs. normal samples by immunofluorescence staining. The relative expressions (green fluorescence intensity vs. blue fluorescence intensity) of CXCL9, 10 (IP10), CXCL11 and 13 (BCA1) as well as DAPI in TNBC and NATs were quantified using ImageJ (×64, version 1.8.0). The "ns", "*", and "**" indicate statistical significance at $p>0.05$, $p<0.05$, and $p<0.01$, respectively.

DSP assay of clinical specimens

DSP of TNBC tissues and NATs was conducted to uncover the immune infiltration in TNBC (Figure 5A). In total, 24 ROIs (14 ROIs in TNBC tissues and 10 ROIs in NATs) were selected (Figure 5B).

Considering that normalizers should correlate ROIs and be unrelated to the underlying biology, correlations between histone H3, S6, GAPDH, and IgG background control probes were analyzed to select the normalization method (Figure 5C). Each pair exhibited a high Pearson coefficient. IgG was selected as the normalizer across ROIs. Both principal component analysis (PCA) and heatmap hierarchical clustering revealed that ROIs could be roughly clustered into two groups (Figure 5D and E).

Immune-related DEPs were subsequently evaluated in TNBC tissues compared to normal tissues (NTs, Figure 5F). Most immune-related proteins, except CD20, PD-1 (an immunosuppressive molecule), and CD56, were up-regulated in TNBC tissues vs. NATs, indicating immune infiltration in TNBC. The up-regulation of PD-L1 indicated that patients with TNBC could receive immunotherapy and benefit from it.

Discussion

Building an accurate prognostic ranking system is imperative due to the poor therapeutic outcomes and prognosis of patients with TNBC, highlighting the significance of personalized treatment. In this study, we observed a correlation between immune and hypoxia status and the survival of patients with TNBC. Consequently, we developed a prognostic model comprising 11 immune-hypoxia genes, whose efficacy in predicting the prognosis of patients with

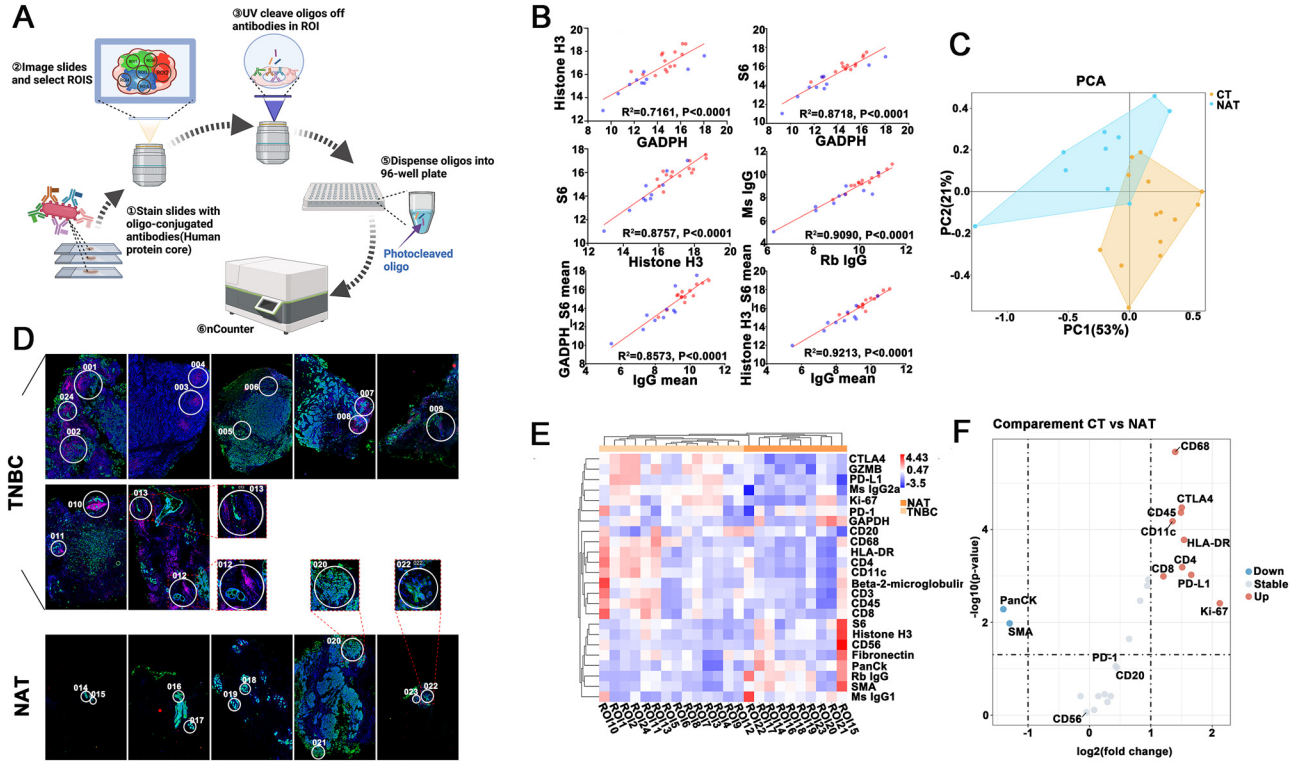

Figure 5: DSP analysis of CTs vs. NATs. (A) The process of DSP. (B) ROIs selection in TNBC CTs and NATs. ROIs were selected according to immunofluorescence staining for PanCK (green), CD45 (red), and DAPI (blue). A total of 24 ROIs were selected from each tumor (14 in CTs, and 10 in NATs). (C) Evaluation of housekeeping proteins and IgG as normalizers. (D) PCA analysis of normalized protein levels in CTs and NATs. (E) Clustered heatmap of relative protein levels per ROI. (F) The volcano map shows nine significantly up-regulated proteins and two significantly down-regulated proteins (CTs vs. NATs).

TNBC was validated across multiple cohorts, including cohort GSE202203, GSE103091, and TCGA. Additionally, we demonstrated the importance of CXCL9, 10, 11, and 13 as chemokines strongly associated with hypoxia and immune status, showing differential expression between high- and low-risk groups in TNBC.

Few studies have explored the correlation between immunity and hypoxia in TNBC TME [32, 33]. Ma et al. provided evidence that hypoxia suppresses immune effector activity through epigenetic reprogramming in TNBC [32]. Hypoxia, coupled with continuous antigen stimulation, plays a crucial role in inducing immune exhaustion and resistance to immunotherapy. In our study, we investigated hypoxia-immune-associated genes in TNBC, identifying prognostically relevant hypoxia-immune-associated DEGs, primarily risk genes. From these, we selected 11 DEGs to obstruct a prognostic model. The results of ssGSEA indicated higher immune infiltration levels in the low-risk group, whereas T cell exclusions, M2 TAM infiltration, and MDSC levels were higher in the high-risk group, suggesting poorer immunotherapy efficacy in the latter. The ability of the hypoxic TME to promote tumor progression by modulating the immune response was highlighted. Our results provide unique biomarkers for predicting immune efficacy, offering original and efficient insights.

DSP represents a novel method for high-plex digital quantification of proteins in clinical tissues. A previous study demonstrated the up-regulation of immune cell markers HLA-DR, CD11c, PD-1, CD3, CD4, ICOS CD278, and CD45RD in epithelial vs. stromal compartments in TNBC [34]. Our DSP results indicated the infiltration of macrophages (CD68), CD8 T cells (CD8) and CD4 T cells (CD4). Recent studies have reported immune infiltration in the TNBC TME [34–36]. **Xiao et al.** categorized TNBC microenvironment phenotypes into three heterogeneous clusters with distinct potential immune escape mechanisms [35]. Combining spatial resolution of immune cells with laser capture microdissection gene expression profiles, infiltration of granzyme B+CD8+T cells (GzmB+CD8+T cells) in TNBC was demonstrated [36]. Although some studies have focused on the immune infiltration in TNBC, further research is required to explore the underlying mechanisms.

Protective DEGs were notably enriched in chemokine signaling pathways and cytokine–cytokine receptor interaction, with a particular emphasis on the CXC chemokine subfamily. CXC chemokines play a crucial role in regulating the migratory patterns and positioning of immune cells. Among them, CXCL9, 10, 11, and 13 exhibited strong correlations with model genes and demonstrated differential expression between high- and low-risk groups. These chemokines are particularly noteworthy for their ability to recruit tumor-suppressive lymphocytes, such as cytotoxic T cells or NK cells, into solid tumors [37]. Additionally, they also exert an angiostatic effect via the CXCR3 receptor [38]. CXCL13 is the first chemokine identified with a selective chemotactic effect on B cells, also exhibits migratory effects on T cells and macrophages [39, 40]. CXCR5, initially called as BLR1, serves as the receptor for CXCL13 [41]. In TNBC, our analysis of transcriptome data from TCGA, qRT-PCR (except CXCL13), and immunofluorescence staining assays revealed differential expression of CXCL2, 9, 10, and 13 in CTs vs. NATs. These chemokines showed positive correlations with the infiltration of most immune cells in TNBC. Moreover, CXCL9 and CXCL13 displayed negative correlations with hypoxia.

While the CXCLs discussed in our study demonstrated potential predictive effects for immune efficacy in TNBC, there are several limitations to consider. The restricted availability of tissues hindered additional verification efforts. However, despite these limitations, the distinct insights gained in TNBC present strong clinical guidance potential. Additionally, the interactions between CXCL9, 10, 11, and 13 with their receptors remain unclear. Future collaborative efforts with multiple institutions will be pursued to investigate these.

Conclusions

In conclusion, this study revealed that the of immune and hypoxia status was intricately linked to the prognosis of patients with TNBC with notable influence from CXCL9, 10, 11, and 13. The developed prognostic model, based on 11 characteristic genes, offers a new and accurate tool for predicting the prognosis of patients with TNBC. CXCL9, 10, 11, and especially CXCL13 emerge as potential targets to modulate the hypoxia and immune status of the TNBC TME, potentially transitioning it from a high-risk to a low-risk status.

Research ethics: This study was conducted according to the guidelines laid down in the Declaration of Helsinki and all procedures involving human participants were approved by the Human Research Ethics Committee at the University of Zhejiang Cancer Hospital Ethics Committee (No.IRB-2021-19).
Informed consent: After an adequate explanation of the study, informed consents were obtained from patients.
Author contributions: Jingkui Tian, Wei Zhu, Yue Feng, Shouxin Li and Vinesh Maharaj aided in writing the manuscript. Luping Wang, Zhuo Han, Xiying Shao, Haote Han and Jiahui Ma designed the study and assisted in writing the manuscript. Luping Wang edited the manuscript. All authors read and approved the final manuscript.
Competing interests: The authors declare that the research was conducted in the absence of any commercial or financial relationships that could be construed as a potential conflict of interest.
Research Funding: This work was supported by Key R&D Program of Zhejiang [No. 2022C03053] to Jingkui Tian.
Data availability: Not applicable.

References

1. Siegel RL, Miller KD, Wagle NS, Jemal A. Cancer statistics, 2023. CA Cancer J Clin 2023;73:17–48.
2. Katsura C, Ogunmwonyi I, Kankam HK, Saha S. Breast cancer: presentation, investigation and management. Br J Hosp Med 2022;83:1–7.
3. Fan S, Yang Z, Ke Z, Huang K, Liu N, Fang X, et al. Downregulation of the long non-coding RNA TUG1 is associated with cell proliferation, migration, and invasion in breast cancer. Biomed Pharmacother 2017; 95:1636–43.
4. Keenan TE, Tolaney SM. Role of immunotherapy in triple-negative breast cancer. J Natl Compr Canc Netw 2020;18:479–89.
5. Nolan E, Lindeman GJ, Visvader JE. Deciphering breast cancer: from biology to the clinic. Cell 2023;186:1708–28.
6. Ye F, Dewanjee S, Li Y, Jha NK, Chen ZS, Kumar A, et al. Advancements in clinical aspects of targeted therapy and immunotherapy in breast cancer. Mol Cancer 2023;22:105.
7. Nagini S. Breast cancer: current molecular therapeutic targets and new players. Anti Cancer Agents Med Chem 2017;17:152–63.
8. Prat A, Pineda E, Adamo B, Galván P, Fernández A, Gaba L, et al. Clinical implications of the intrinsic molecular subtypes of breast cancer. Breast 2015;24:S26–35.
9. Singh DD, Yadav DK. TNBC: potential targeting of multiple receptors for a therapeutic breakthrough, nanomedicine, and immunotherapy. Biomedicines 2021;9:876.
10. Semenza GL. Targeting intratumoral hypoxia to enhance anti-tumor immunity. Semin Cancer Biol 2023;96:5–10.
11. Cao Y, Langer R, Ferrara N. Targeting angiogenesis in oncology, ophthalmology and beyond. Nat Rev Drug Discov 2023;22:476–95.
12. Chiu DK, Tse AP, Xu IM, Cui JD, Lai RK, Li LL, et al. Hypoxia inducible factor HIF-1 promotes myeloid-derived suppressor cells accumulation through ENTPD2/CD39L1 in hepatocellular carcinoma. Nat Commun 2017;8:517.
13. Korbecki J, Olbromski M, Dzięgiel P. CCL18 in the progression of cancer. Int J Mol Sci 2020;21:7955.
14. Shi Y, David JR, Shen J. The role of the CXCL12/CXCR4/CXCR7 chemokine Axis in cancer. Front Pharmacol 2020;11:574667.

15. Wu T, Yang W, Sun A, Wei Z, Lin Q. The role of CXC chemokines in cancer progression. Cancers 2022;15:167.
16. Fernandez-Avila L, Castro-Amaya AM, Molina-Pineda A, Hernández-Gutiérrez R, Jave-Suarez LF, Aguilar-Lemarroy A. The value of CXCL1, CXCL2, CXCL3, and CXCL8 as potential prognosis markers in cervical cancer: evidence of E6/E7 from HPV16 and 18 in chemokines regulation. Biomedicines 2023;11:2655.
17. Addison CL, Daniel TO, Burdick MD, Liu H, Ehlert JE, Xue YY, et al. The CXC chemokine receptor 2, CXCR2, is the putative receptor for ELR+CXC chemokine-induced angiogenic activity. J Immunol 2000;165:5269–77.
18. Zhou C, Gao Y, Ding P, Wu T, Ji G. The role of CXCL family members in different diseases. Cell Death Discov 2023;9:212.
19. Edderkaoui B. Chemokines in cartilage regeneration and degradation: new insights. Int J Mol Sci 2023;25:381.
20. Korbecki J, Bosiacki M, Barczak K, Łagocka R, Brodowska A, Chlubek D, et al. Involvement in tumorigenesis and clinical significance of CXCL1 in reproductive cancers: breast cancer, cervical cancer, endometrial cancer, ovarian cancer and prostate cancer. Int J Mol Sci 2023;24:7262.
21. Motyka J, Kicman A, Kulesza M, Ławicki S. CXC ELR-positive chemokines as diagnostic and prognostic markers for breast cancer patients. Cancers 2023;15:3118.
22. Hara T, Tanegashima K. Pleiotropic functions of the CXC-type chemokine CXCL14 in mammals. J Biochem 2012;151:469–76.
23. Liu Q, Li A, Tian Y, Wu JD, Liu Y, Li T, et al. The CXCL8-CXCR1/2 pathways in cancer. Cytokine Growth Factor Rev 2016;31:61–71.
24. Guo F, Long L, Wang J, Wang Y, Liu Y, Wang L, et al. Insights on CXC chemokine receptor 2 in breast cancer: an emerging target for oncotherapy. Oncol Lett 2019;18:5699–708.
25. Xu C, Zhao H, Chen H, Yao Q. CXCR4 in breast cancer: oncogenic role and therapeutic targeting. Drug Des Dev Ther 2015;9:4953–64.
26. Roberto M, Arrivi G, Di Civita MA, Barchiesi G, Pilozzi E, Marchetti P, et al. The role of CXCL12 axis in pancreatic cancer: new biomarkers and potential targets. Front Oncol 2023;13:1154581.
27. Łabędź W, Przybyla A, Zimna A, Dąbrowski M, Kubaszewski Ł. The role of cytokines in the metastasis of solid tumors to the spine: systematic review. Int J Mol Sci 2023;24:3785.
28. Marin JA, Kimbrough EO, Manochakian R, Zhao Y, Lou Y. Immunotherapies targeting stimulatory pathways and beyond. J Hematol Oncol 2021;14:78.
29. Mishra A, Suman KH, Nair N, Majeed J, Tripathi V. An updated review on the role of the CXCL8-CXCR1/2 axis in the progression and metastasis of breast cancer. Mol Biol Rep 2021;48:6551–61.
30. Fu J, Li K, Zhang W, Wan C, Zhang J, Jiang P, et al. Large-scale public data reuse to model immunotherapy response and resistance. Genome Med 2020;12:21.
31. Livak KJ, Schmittgen TD. Analysis of relative gene expression data using real-time quantitative PCR and the 22DDCT method. Methods 2001;25:402–8.
32. Ma S, Zhao Y, Lee WC, Ong L, Lee PL, Jiang Z, et al. Hypoxia induces HIF1α-dependent epigenetic vulnerability in triple negative breast cancer to confer immune effector dysfunction and resistance to anti-PD-1 immunotherapy. Nat Commun 2022;13:4118.
33. Giatromanolaki A, Gkegka AG, Pouliliou S, Biziota E, Kakolyris S, Koukourakis M. Hypoxia and anaerobic metabolism relate with immunologically cold breast cancer and poor prognosis. Breast Cancer Res Treat 2022;194:13–23.
34. Stewart RL, Matynia AP, Factor RE, Varley KE. Spatially-resolved quantification of proteins in triple negative breast cancers reveals differences in the immune microenvironment associated with prognosis. Sci Rep 2020;10:6598.
35. Xiao Y, Ma D, Zhao S, Suo C, Shi J, Xue M, et al. Multi-omics profiling reveals distinct microenvironment characterization and suggests immune escape mechanisms of triple-negative breast cancer. Clin Cancer Res 2019;25:5002–14.
36. Gruosso T, Gigoux M, Manem VSK, Bertos N, Zuo D, Perlitch I, et al. Spatially distinct tumor immune microenvironments stratify triple-negative breast cancers. J Clin Invest 2019;129:1785–800.
37. Bronger H, Magdolen V, Goettig P, Dreyer T. Proteolytic chemokine cleavage as a regulator of lymphocytic infiltration in solid tumors. Cancer Metastasis Rev 2019;38:417–30.
38. Chan TYH, Wong JSY, Kiang KM, Sun CWY, Leung GK. The duality of CXCR3 in glioblastoma: unveiling autocrine and paracrine mechanisms for novel therapeutic approaches. Cell Death Dis 2023;14:835.
39. Heeger PS, Haro MC, Jordan S. Translating B cell immunology to the treatment of antibody-mediated allograft rejection. Nat Rev Nephrol 2024. https://doi.org/10.1038/s41581-023-00791-0 [Epub ahead of print].
40. Harada T, Kikushige Y, Miyamoto T, Uno K, Niiro H, Kawakami A, et al. Peripheral helper-T-cell-derived CXCL13 is a crucial pathogenic factor in idiopathic multicentric Castleman disease. Nat Commun 2023;14:6959.
41. Drouillard D, Craig BT, Dwinell MB. Physiology of chemokines in the cancer microenvironment. Am J Physiol Cell Physiol 2023;324:C167–82.

Supplementary Material: This article contains supplementary material (https://doi.org/10.1515/oncologie-2023-0539).